

Optimization of a Thermal Lens Microscope for Detection in a Microfluidic Chip

Mingqiang Liu · Uroš Novak · Igor Plazl · Mladen Franko

Received: 15 April 2013 / Accepted: 2 September 2013 / Published online: 26 September 2013
© Springer Science+Business Media New York 2013

Abstract The optical configuration of a thermal lens microscope (TLM) was optimized for detection in a microfluidic chip with respect to the flow velocity, and the pump and probe beam parameters (beam waists, offsets, and mode mismatching degree). It was found that an appropriate pump–probe beam offset for a certain flow velocity would provide not only a higher sensitivity but also a better response linearity of TLM over three orders of magnitude of sample concentration. Diffraction-limited pump beam excitation is advantageous for space-resolved measurement, while a larger pump beam with 10 times lower power density is favorable for higher sensitivity at given experimental conditions. As an application, TLM was used to study the diffusion of azobenzene in a microfluidic chip. Diffusion profiles at different distances from the mixing point were recorded by scanning the TL signal along the cross section of the microchannel. By fitting the diffusion profiles to a theoretical model of mass transfer in a microchannel, diffusion coefficients of azobenzene in octane and methanol were determined to be $5 \times 10^{-10} \text{ m}^2 \cdot \text{s}^{-1}$ and $6 \times 10^{-10} \text{ m}^2 \cdot \text{s}^{-1}$, respectively.

Keywords Diffusion measurement · Microfluidic chip · Optimization · Thermal lens microscope

M. Liu (✉) · M. Franko
Laboratory for Environmental Research, University of Nova Gorica, Vipavska 13,
P.O. Box 301, 5000 Nova Gorica, Slovenia
e-mail: mingqiang.liu@yahoo.com

U. Novak · I. Plazl
Department of Chemical Engineering, Faculty of Chemistry and Chemical Technology,
University of Ljubljana, Askercева 5, 1000 Ljubljana, Slovenia

1 Introduction

A thermal lens microscope (TLM) [1] is a recent promising development of thermal lens spectrometry (TLS) toward miniaturization and automation. A TLM not only has the similar advantage of high sensitivity as the conventional TLS [2], but also has its unique characteristics such as high temporal (\sim ms) and spatial resolutions (\sim μ m), which enable it for high-sample-throughput and small-volume detection of a variety of compounds with low sample/reagent consumption when it is coupled to lab-on-chip chemistry [3], such as in microfluidic chips or miniaturized microtiter plates. It has already been successfully applied for analysis of trace cobalt concentrations with a limit of detection (LOD) of 0.13 zmol (zeptomole) [4] or carbamate pesticide derivatives with an LOD of 7×10^{-8} M (molar) [5], and the analysis time was reduced from the usual 2 h to 3 h in a conventional cell to only 50 s in a microfluidic chip. It has also been used for imaging of the human leukocyte antigen on the membrane of a mononuclear leukocyte [6] and cytochrome c in a biological cell before and after apoptosis [7].

Optimizations of the optical scheme of TLS instruments have been done by some researchers. For higher sensitivity, Proskurnin et al. [8] optimized the TLM configuration and obtained LODs of $5.96 \mu\text{g} \cdot \text{L}^{-1}$ and $1.81 \mu\text{g} \cdot \text{L}^{-1}$ for ferroin and Sunset Yellow at 488.0 nm, respectively. Chanlon and Georges [9] described the effect of the flow rate on the TL signal within a capillary tube for a pulsed-laser crossed-beam TLS. Impacts of the liquid flow on the TL signal of photolabile compounds were mentioned as well in some papers [10, 11]. Though these optimizations are very useful, a detailed analysis of the influence of the liquid flow on the TL signal in a microfluidic channel is still lacking.

In this paper, an analysis of the impacts of the sample flow in a microfluidic channel on the TL signal is made both theoretically and experimentally for a TLM setup built in the laboratory. The flow-induced probe beam noise was checked at different flow velocities. Correspondingly, the optical configuration of the TLM was optimized for the best signal-to-noise ratio. As an application, the diffusion of azobenzene in one-phase and two-phase systems in a microreactor chip was investigated by the optimized TLM.

2 Theory

The theoretical model of TLS in a flowing medium based on the Fresnel diffraction theory has been presented in our previous work [12]. Here, a brief description of this model is given. In Fig. 1, a schematic diagram of the optical configuration of a laser-excited TLM in a microchannel is shown. The flow profile in the microchannel is actually laminar, but in theory, to obtain an analytic temperature distribution, the flow velocity across the channel cross section is assumed to be homogeneous. When the sample flow is in the x direction, this homogeneous flow velocity is denoted by v_x , which is half the maximum flow velocity of the laminar flow.

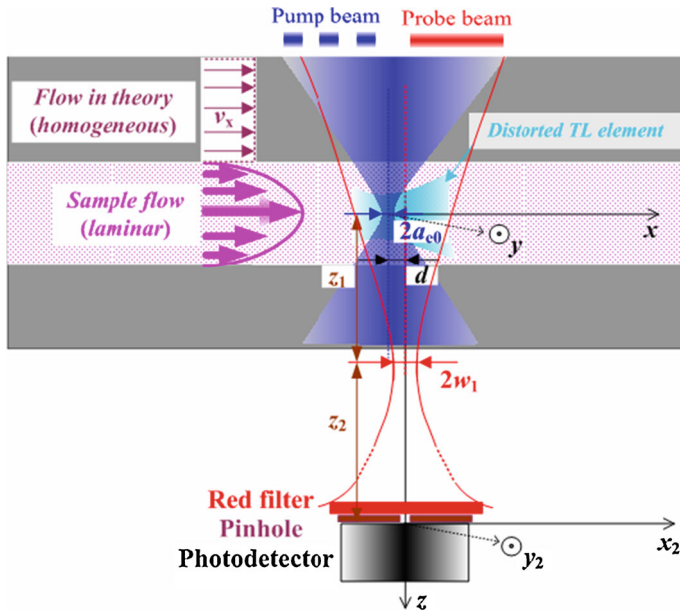


Fig. 1 Schematic diagram of the optical configuration of a TLM system in a microchannel

The temperature distribution in the sample can be written as

$$\begin{aligned}
 T(x, y, t) &= \frac{\alpha P D}{\pi k} \int_0^t \frac{(1 + \cos \omega \tau) \exp \left\{ -2 \left[(x - v_x(t - \tau))^2 + y^2 \right] / \left[8 D(t - \tau) + a_{e0}^2 \right] \right\} d\tau}{8 D(t - \tau) + a_{e0}^2}, \tag{1}
 \end{aligned}$$

where α , k , and D are the absorption coefficient, thermal conductivity, and thermal diffusivity of the sample, respectively. P , a_{e0} , and ω ($= 2\pi f$ with f the modulation frequency) are the power, beam waist radius, and angular modulation frequency of the pump laser, respectively. With the sample flows through the detection site of the TLM, the temperature profile shifts in the direction of the flow and correspondingly, the TL element is distorted, which consequently decreases the TL signal. To alleviate the flow-induced signal reduction, the probe beam should be displaced downstream (or the pump beam be displaced upstream) a certain distance to fit the change of the temperature distribution. This distance is called the pump–probe beam offset (denoted by d in Fig. 1), which is different with respect to different flow velocities.

On the basis of the Fresnel diffraction theory, the complex electric field distribution of the probe beam in the detection plane can be expressed as

$$E_2(x_2, y_2, d, z_1 + z_2, t) = \frac{j \exp(-jkz_2)}{2\lambda z_2}$$

$$\int_{-\infty}^{+\infty} \int_{-\infty}^{+\infty} E_1'(x, y, d, z_1, t) \exp \left\{ -\frac{jk}{2z_2} [(x_2 - x)^2 + (y_2 - y)^2] \right\} dx dy, \quad (2)$$

in which λ and $k = 2\pi/\lambda$ are the wavelength and the wave number of the probe beam, respectively. z_1 and z_2 are the distance from the probe beam waist (w_1) to the sample and the distance from the sample to the detection plane, respectively. (x, y) and (x_2, y_2) are the coordinates in the sample and detection plane, respectively. $E_1'(x, y, d, z_1, t)$ is the complex amplitude of the electric field of the probe beam at the exit plane of the TL element:

$$E_1'(x, y, d, z_1, t) = E_1(x, y, z_1) \exp[-j\Delta\phi(x - d, y, t)]. \quad (3)$$

$E_1(\cdot)$ and $\Delta\Phi(\cdot)$ are the electric field of the probe beam before the TL element and the phase change induced by the TL element, respectively. For a Gaussian probe beam with the TEM00 mode, $E_1(\cdot)$ can be found in Ref. [12]. The phase shift is given as

$$\Delta\phi(x - d, y, t) = \frac{2\pi}{\lambda} l \frac{dn}{dT} T(x - d, y, t), \quad (4)$$

where l denotes the effective sample length (or the thickness of the TL element), and dn/dT is the temperature coefficient of the refractive index of the sample. When using a photodiode placed behind a pinhole to measure the axial density of the probe beam, the TL signal S can be defined as

$$S = \frac{|S_{ac}|}{S_{dc}} = \frac{|I_2(t = n2\pi/\omega + \pi/\omega) - I_2(t = n2\pi/\omega)|}{I_2(t = 0)}, \quad (5)$$

where $I_2(\cdot)$ is the intensity obtained by taking the complex square of the electric field; S_{ac} is the intensity change of the probe beam in a modulation cycle; n is an arbitrary cycle in the steady state; and S_{dc} is the central intensity of the probe beam before excitation.

3 Experiments and Discussion

Figure 2 shows the laser-excited TLM coupled with a microfluidic system built in the lab. A pump beam from an argon laser (Innova 90, Coherent) at 457.9 nm is reflected by mirrors to the beam expander II (lenses L3 and L4 with focal lengths of 3 cm and 5 cm, respectively), and then after passing a mechanical chopper working at 1.03 kHz, it is combined by a dichroic mirror with a probe beam from a He-Ne laser (632.8 nm, 25-LHP-151-230, Melles Griot) which first passes an optical isolator (composed of a linear polarizer and a quarter wave plate) and the beam expander I (composed of lenses L1 and L2 with focal lengths of 4 cm and 15 cm, respectively). These two beams are aligned coaxially through an objective lens [$20\times$ /NA (Numerical Aperture) 0.40], and then propagated through a microfluidic chip (a microreactor chip with a microchannel $220\ \mu\text{m}$ wide \times $50\ \mu\text{m}$ deep, Micronit Microfluidics) where the

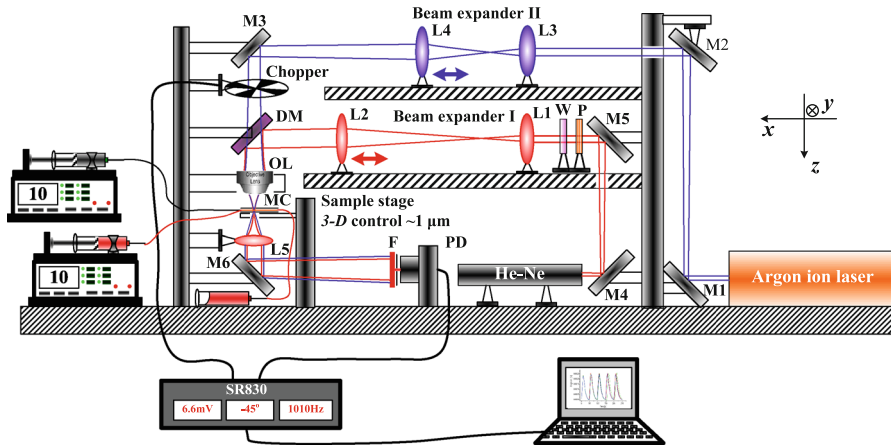


Fig. 2 Schematic diagram of a laser-excited TLM coupled with a microfluidic system. M1–M6: mirrors; L1–L5: lenses; DM: dichroic mirror; OL: objective lens; MC: microfluidic chip; W: $\lambda/4$ waveplate at 632.8 nm; P: linear polarizer; F: interference filter at 632.8 nm; PD: photodiode

TL effect is generated. The probe beam is diffracted by the TL effect, and after a condenser lens, its axial intensity is monitored by a photodiode (PDA36A, Thorlabs) mounted behind a pinhole. Double-arrow lines in the figure mean that the components can be moved forward and backward. The microfluidic system is composed of two microsyringe pumps (NE-1000, Newera Pump Systems), a microchip, a waste syringe, and connecting tubings. Flow rates of $0 \mu\text{L} \cdot \text{min}^{-1}$ to $50 \mu\text{L} \cdot \text{min}^{-1}$ (corresponding to flow velocities of $0 \text{ mm} \cdot \text{s}^{-1}$ to $80 \text{ mm} \cdot \text{s}^{-1}$ in the microchannel) were used. At first, the ferroin solution was used as the sample for optimizing the TLM system. In Sects. 3.1 to 3.3, the concentration of the ferroin solution is $300 \mu\text{M}$ (micromolar), and the excitation power is 10 mW.

3.1 Dependence of TL Signal on the Probe-to-Pump Beam Radius Ratio

In Fig. 3, the TL signals as a function of the probe-to-pump beam radius ratio $\{w_s/a_{e0}\}$, the square root of mode-mismatching degree $m = (w_s/a_{e0})^2$ [12] at $v_x = 0$ and $52 \text{ mm} \cdot \text{s}^{-1}$ are shown. w_s is the probe beam radius in the sample, which for a Gaussian beam with the TEM₀₀ mode, is defined as $w_s = w_1[1 + (z_1/z_R)^2]^{1/2}$ with $z_R (= \pi w_1^2/\lambda)$ the Rayleigh range of the probe beam. In w_s , z_1 's was varied as follows: first, a position of $z_1 = 0$ where the TL signal achieved a minimum was found and the corresponding distance d between L1 and L2 (Fig. 2) was 23.5 cm; then, different z_1 's from $0 \mu\text{m}$ to $160 \mu\text{m}$ were obtained by moving lens L2 from 23.5 cm to 18.2 cm. w_1 changed only slightly (from $1 \mu\text{m}$ to $1.12 \mu\text{m}$). Due to the difficulty of measuring z_1 in the experiment, values of z_1 were theoretically calculated by the matrix optics method for a Gaussian beam with respect to the change of d from 23.5 cm to 18.2 cm. The probe beam waist radius and the pump beam waist radius were determined to be $1 \mu\text{m}$ and $2 \mu\text{m}$, respectively, by fitting the probe or pump beam radii (determined by the knife-edge method) along the optical axis under the OL to the Gaussian beam propagation profile. For $v_x = 52 \text{ mm} \cdot \text{s}^{-1}$, the TL signals at $d = 0, d_{\text{opt}+}$ and

Fig. 3 TL signal of ferroin as a function of probe-to-pump beam radius ratio at $v_x = 0$ and $52 \text{ mm} \cdot \text{s}^{-1}$. a_{e0} is $2 \mu\text{m}$

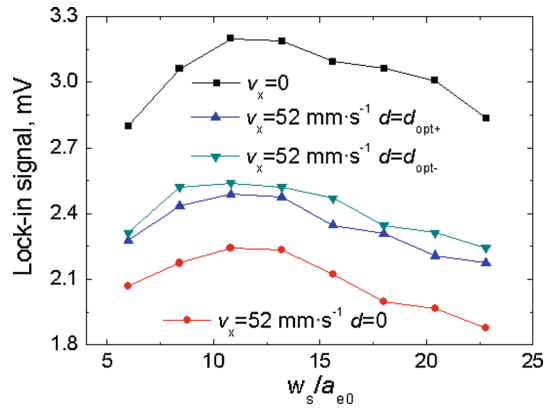
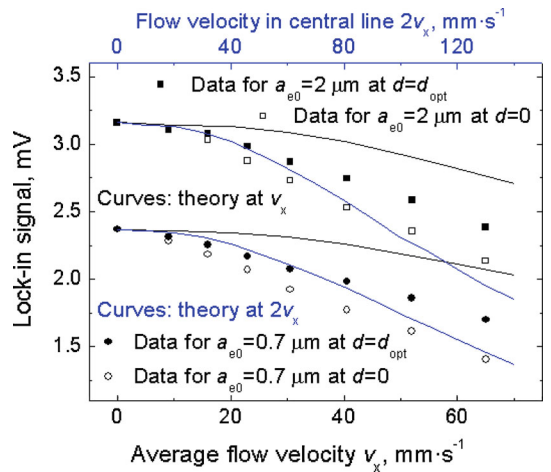


Fig. 4 TL signal as a function of flow velocity in the microchannel for two pump beam profiles at two pump-probe beam offsets



d_{opt-} were measured. Here, d_{opt+} is the optimum beam offset when the flow runs from the carrier reservoir to the waste reservoir and d_{opt-} when the flow is reversed. To realize such an offset (d_{opt+} or d_{opt-}) between the pump and probe beams, the pump beam was shifted by d_{opt+} or d_{opt-} along the direction opposite to the sample flow. From the figure we can see that at $v_x = 52 \text{ mm} \cdot \text{s}^{-1}$, the maximum TL signal at d_{opt} is about 1.11 times larger than that at $d = 0$. The small difference between the TL signals at d_{opt+} and d_{opt-} indicates the imperfect symmetry of the probe beam in the detection plane, and the improvement to the TL signal seems a little bit better at $d = d_{opt-}$ than that at $d = d_{opt+}$. A probe-to-pump beam radius ratio of 12 was chosen for the next experiments.

3.2 Dependence of TL Signal on the Flow Velocity

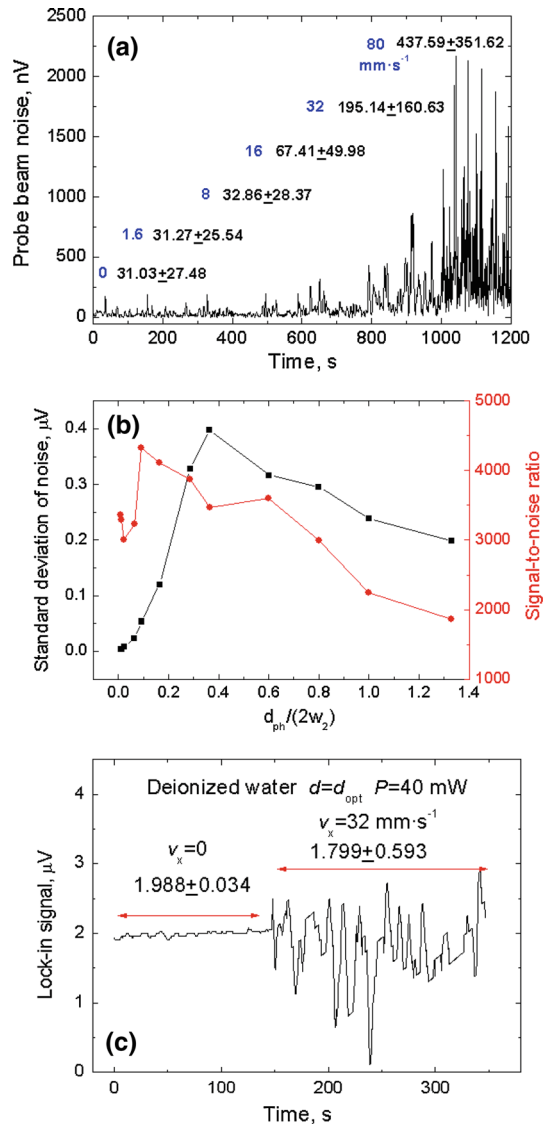
In Fig. 4, the TL signals as a function of the flow velocity in the microchannel for two pump beam waist radii of $0.7 \mu\text{m}$ and $2 \mu\text{m}$ are shown. The signals were measured at

the beam offsets of 0 and d_{opt} . The theoretical curves were calculated for the average flow velocity v_x in the cross section of the microchannel and for the maximal flow velocity in a microchannel, which for laminar flows is $2v_x$ in the central axis of the microchannel. Only the theoretical curves at d_{opt} were given for clearness. From the figure we can see that the measured TL signal decreases faster with the flow velocity than the theoretical prediction at v_x but slower than that at $2v_x$. The change of TL signals for $a_{e0} = 0.7 \mu\text{m}$ at d_{opt} is closer to the theory at $2v_x$ in comparison with the case of $a_{e0} = 2 \mu\text{m}$. This is because a big part of the TL signal ($>50\%$) is generated within the confocal distance ($z_c = 2z_R$) of the pump laser, which is located around the central axis of the microchannel, and the confocal distance at $a_{e0} = 0.7 \mu\text{m}$ is much smaller than that at $a_{e0} = 2 \mu\text{m}$. On the other hand, we can see that the TL signal at $a_e = 2 \mu\text{m}$ is about 1.4 times higher than that at $a_e = 0.7 \mu\text{m}$. This means that though diffraction-limited excitation ensures a better spatial resolution, a higher detection sensitivity can be achieved at a larger pump beam waist radius. It should be noted that this conclusion is obtained for given systematic parameters of this laser-excited TLM (sample length of $50 \mu\text{m}$, modulation frequency of 1.03 kHz, pump laser power of 10 mW, probe beam waist radius of $1 \mu\text{m}$, probe-to-pump beam radius ratio of 12 in the sample, detection distance of 5 cm). Changing of some parameters, such as increasing the modulation frequency and/or decreasing the sample length would result in a higher sensitivity at a smaller pump beam waist radius. At low flow velocities, such as $v_x < 10 \text{ mm} \cdot \text{s}^{-1}$, the detection scheme can be kept unchanged, but if the flow velocity increases to a high value (such as above $20 \text{ mm} \cdot \text{s}^{-1}$), it is necessary to readjust the detection scheme to achieve the maximum TL signal.

3.3 Influence of Flow-Induced Noise on TLS Measurement

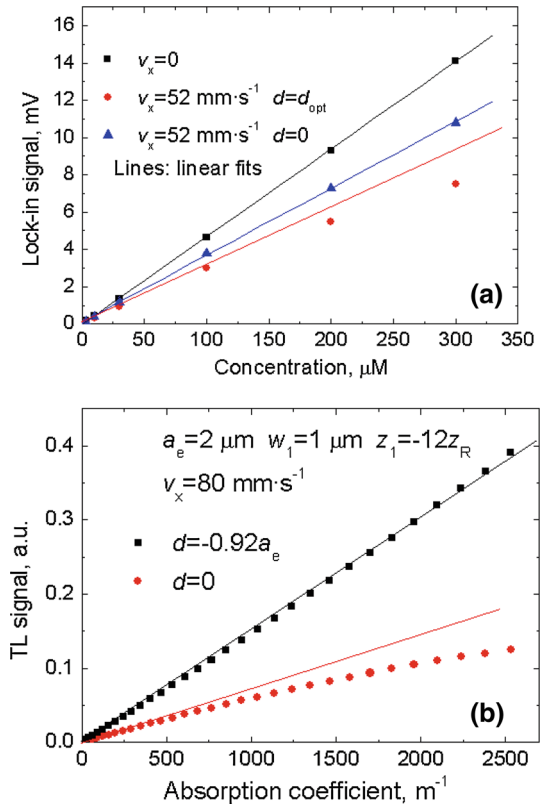
Liquid flow in the microchannel deteriorates the TL signal from different aspects: one is that the flow moves the heat out of the detection area, which decreases the TL signal amplitude, as shown in Fig. 4. Another aspect is the fluctuation of the flow of the liquid, which not only makes the TL element unstable, but also interferes with the probe beam even if there is no pump beam excitation. As shown in Fig. 5a, when the pump beam was blocked, the standard deviation of the probe beam noise at different flow velocities was checked. The figure shows that when the flow velocity is less than $16 \text{ mm} \cdot \text{s}^{-1}$, there is slight deterioration of the probe beam noise, but at higher flow velocities, the deterioration becomes very obvious. This deterioration comes from the disturbance of the liquid flow on the propagation of the probe beam through the microchannel, which can be induced by the fluctuation of the flow and/or the presence of some kind of micro- or nanobubbles in the fluid. The flow-induced noise behaves like the noise caused by the beam pointing instability of the light source. As indicated by the black curve in Fig. 5b, the probe beam noise varies with the pinhole aperture-to-beam size ratio [$d_{\text{ph}}/(2w_2)$] in a way similar to the case of beam pointing instability-induced noise (Fig. 1 in Ref. [13]) except for less pronounced decreasing of the noise at large $d_{\text{ph}}/(2w_2)$. This is because in comparison to the beam pointing instability-induced

Fig. 5 (a) Probe beam noise at different flow velocities at $d_{ph}/(2w_2)$ of 0.3 when the pump beam is blocked, (b) probe beam noise and signal-to-noise ratio as a function of $d_{ph}/(2w_2)$ at flow velocity of $32 \text{ mm} \cdot \text{s}^{-1}$, and (c) TL signal of deionized water at flow velocities of $0 \text{ mm} \cdot \text{s}^{-1}$ and $32 \text{ mm} \cdot \text{s}^{-1}$ (Color figure online)



noise only, there are other noises such as flicker and shot noises in the noise curve in Fig. 5b, in which the shot noise becomes the major noise source at large $d_{ph}/(2w_2)$. Correspondingly, as predicted in Fig. 1 in Ref. [13] that the signal-to-noise ratio would not change with $d_{ph}/(2w_2)$ if only the beam pointing instability-induced noise exist in the TLS system, the signal-to-noise ratio (red curve, Fig. 5b) does not change a lot (<35 %, which is probably due to measurement error) at relatively small $d_{ph}/(2w_2)$ (such as <0.6) where the flow-induced noise dominates and then decreases at large $d_{ph}/(2w_2)$ where the shot noise is dominant. From the figure we can see that in flow-induced noise-limited TLS experiments,

Fig. 6 (a) TL signal linearity for $v_x = 0 \text{ mm} \cdot \text{s}^{-1}$ and $52 \text{ mm} \cdot \text{s}^{-1}$ and (b) theoretically calculated TL signal as a function of absorption coefficient



$d_{\text{ph}}/(2w_2)$ could be selected between 0.1 and 0.4 for a high signal-to-noise ratio.

3.4 Response Linearity and Detection Limit of TLM

In Fig. 6, response linearities of the TLM in static and flowing modes are presented. The concentration range of ferroin used here is from $3 \mu\text{M}$ to $300 \mu\text{M}$. In the static mode, the signal increases linearly with the concentration of the sample. While for a relatively high flow velocity, as predicted in theory (Fig. 6b), the instrumental response at $d = 0$ is not linear over a relatively large concentration range, a linear response is obtained at $d = d_{\text{opt}}$. Therefore, during the experiment, it is quite desirable to move the pump beam to the optimum position to assure a linear response of the TLM to a certain range of sample concentration, when the flow velocity in the microchannel is relatively high. At an excitation power of 50 mW , the LOD for a $50 \mu\text{m}$ thick ferroin at $v_x = 52 \text{ mm} \cdot \text{s}^{-1}$ is $3 \times 10^{-8} \text{ M}$, corresponding to an absorbance of $1.6 \times 10^{-6} \text{ AU}$ (absorbance unit).

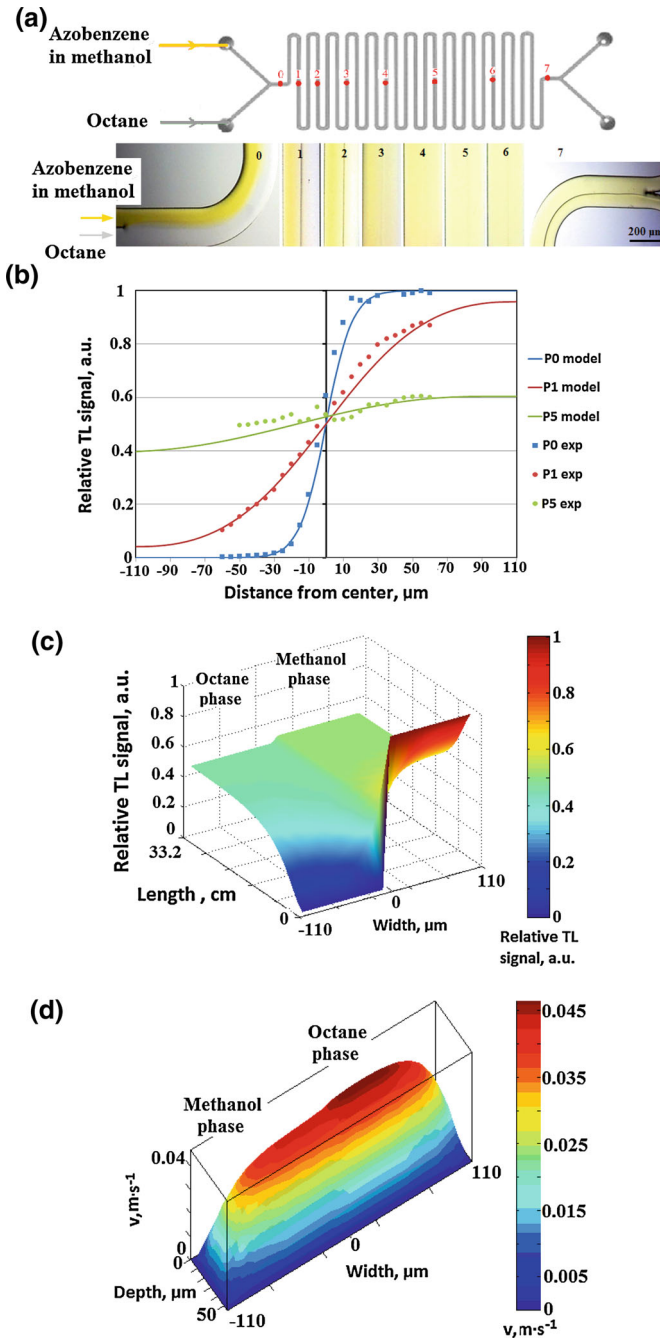


Fig. 7 (a) A picture of azobenzene diffusion from methanol to octane along the microchannel, and relative TL signal profiles (b) at three positions with fitting curves in one-phase system (octane) and (c) in two phases along the entire channel length; and (d) two-phase flow velocity profile in the cross section at a flow rate of $12 \mu L \cdot \text{min}^{-1}$ for octane and of $10 \mu L \cdot \text{min}^{-1}$ for methanol

3.5 Application of TLM to the Study of Molecular Diffusion

By scanning the TL signal in the cross section of the microchannel at different channel positions, the diffusion of molecules in a microspace can be characterized. Here, azobenzene is used as a solute to study the diffusion in one-phase (methanol or octane) or two-phase (methanol/octane) systems.

In Fig. 7, diffusion profiles of azobenzene in one-phase and two-phase systems, as well as the flow velocity profile in two phases, are shown. Symbols of P0–P7 in Fig. 7a denote different positions in the microchannel, which are (0.1, 1, 3, 6, 10, 15, 21, and 30) cm away from the input Y-junction, respectively. Diffusion of azobenzene characterized by the TLM signal is in good agreement with the theoretical model for one-phase or two-phase fluids (Fig. 7b, c). The 3D profiles of the flow and diffusion processes along the microchannel (Fig. 7c, d) were obtained by calculating the momentum and diffusion equation [14], in which both the convection and diffusion terms are considered, with the finite-difference numerical approach in the Matlab code. In Fig. 7d, on account of the difference of physical properties (viscosity and density) between methanol and octane, different flow rates were used for keeping the interface at the middle of the microchannel. Through fitting the experimental data to the model, diffusion coefficients of azobenzene in octane and methanol are determined to be $5 \times 10^{-10} \text{ m}^2 \cdot \text{s}^{-1}$ and $6 \times 10^{-10} \text{ m}^2 \cdot \text{s}^{-1}$, respectively. The partitioning coefficient for azobenzene in the octane/methanol two-phase systems was determined to be 0.92 at 23 °C.

4 Conclusions

From the above discussion, we can see that by optimizing the pump and probe parameters (beam waist radii, mode-mismatching degree, and beam offset) with respect to a certain flow velocity, not only the sensitivity of the TLM but also its response linearity over a certain sample concentration range are improved. Diffraction-limited excitation ensures a better spatial resolution, while at a larger pump beam waist radius, a higher detection sensitivity can be achieved. Low LODs (1.6×10^{-6} AU in a 50 μm channel at 50 mW power) of a TLM-enabled accurate detection of small changes in absorbance, which provides a powerful tool for depicting the governing transport characteristics of an analyte in a microfluidic chip by incorporating a theoretical model of mass transfer in a microchannel.

Acknowledgments The authors thank the Slovenian Research Agency for financial support through the research program grant P1-0034 and the young researcher fellowship to M. Liu.

References

1. M. Harada, K. Iwamoto, T. Kitamori, T. Sawada, *Anal. Chem.* **65**, 2938 (1993)
2. S.E. Bialkowski, *Photothermal Spectroscopy Methods for Chemical Analysis* (Wiley, New York, 1996)
3. T. Kitamori, M. Tokeshi, A. Hibara, K. Sato, *Anal. Chem.* **76**, 52A (2004)
4. M. Tokeshi, T. Minagawa, K. Uchiyama, A. Hibara, K. Sato, H. Hisamoto, T. Kitamori, *Anal. Chem.* **74**, 1565 (2002)

5. A. Smirnova, K. Mawatari, A. Hibara, M.A. Proskurnin, T. Kitamori, *Anal. Chim. Acta* **558**, 69 (2006)
6. H. Kimura, F. Nagao, A. Kitamura, K. Sekiguchi, T. Takehiko, T. Sawada, *Anal. Biochem.* **283**, 27 (2000)
7. E. Tamaki, K. Sato, M. Tokeshi, K. Sato, M. Aihara, T. Kitamori, *Anal. Chem.* **74**, 1560 (2002)
8. M.A. Proskurnin, M.N. Slyadnev, M. Tokeshi, T. Kitamori, *Anal. Chim. Acta* **480**, 79 (2003)
9. S. Chanlon, J. Georges, *Spectrochim. Acta A* **58**, 1607 (2002)
10. N. Ragozina, S. Heissler, W. Faubel, U. Pyell, *Anal. Chem.* **74**, 4480 (2002)
11. K. Mawatari, S. Kubota, T. Kitamori, *Anal. Bioanal. Chem.* **391**, 2521 (2008)
12. M. Liu, D. Korte, M. Franko, *J. Appl. Phys.* **111**, 033109-1 (2012)
13. S.R. Erskine, D.R. Bobbitt, *Appl. Spectrosc.* **42**, 331 (1988)
14. P. Žnidaršič-Plazl, I. Plazl, *Lab Chip* **7**, 883 (2007)